Geophysical Research Letters

RESEARCH LETTER
10.1029/2020GL091252

Amplified Increases of Compound Hot Extremes Over Urban Land in China

Weilin Liao[1], Dan Li[2], Sergey Malyshev[3], Elena Shevliakova[3], Honghui Zhang[4,5], and Xiaoping Liu[1,6]

[1]Guangdong Key Laboratory for Urbanization and Geo-simulation, School of Geography and Planning, Sun Yat-sen University, Guangzhou, China, [2]Department of Earth and Environment, Boston University, Boston, MA, USA, [3]NOAA/Geophysical Fluid Dynamics Laboratory, Princeton, NJ, USA, [4]College of Resources and Environmental Sciences, Hunan Normal University, Changsha, China, [5]Guangdong Guodi Planning Science Technology Co., Ltd., Guangdong, China, [6]Southern Marine Science and Engineering Guangdong Laboratory (Zhuhai), Zhuhai, China

Key Points:

- Both urban and rural summertime hot extremes become more frequent, more intense, and longer lasting in China
- Simulations indicate faster increases of compound hot extremes over urban land than rural land
- Urbanization accelerates the transition of hot extremes from daytime-/nighttime-only events toward compound events

Supporting Information:

- Supporting Information S1

Correspondence to:
X. Liu,
liuxip3@mail.sysu.edu.cn

Citation:
Liao, W., Li, D., Malyshev, S., Shevliakova, E., Zhang, H., & Liu, X. (2021). Amplified increases of compound hot extremes over urban land in China. *Geophysical Research Letters*, *48*, e2020GL091252. https://doi.org/10.1029/2020GL091252

Received 15 OCT 2020
Accepted 9 JAN 2021

Abstract Consecutive hot periods without nighttime heat relief significantly increase mortality and morbidity rates. Using the Geophysical Fluid Dynamics Laboratory land model coupled with a newly developed and validated urban canopy model, changes in three types of summertime hot extremes, that is, independent hot days, independent hot nights, and compound hot events (CHEs), in the 21st century are quantified in China. Results indicate that all three types of hot extremes become more frequent, and CHEs are projected to be the dominant type at the end of this century under the representative concentration pathway 8.5 scenario. Furthermore, compared to the rural land, the urban land experiences even stronger increases in CHEs in terms of frequency, duration, and intensity. These faster increases of CHEs in urban areas highlight the urgency of developing and implementing mitigation and adaptation strategies to combat the adverse health effects of global warming and urban heat islands.

Plain Language Summary As the urban population continues to rise, it is important to quantify the increase of hot extremes over urban areas, which have profound impacts on human health. According to climate simulations and meteorological observations, both urban and rural summertime hot extremes become more frequent, more intense, and longer lasting in China. As the climate warms, hot extremes transition from daytime-/nighttime-only events to compound events, and this transition is accelerated over urban land than rural land. As consecutive hot days without nighttime relief will significantly increase mortality and morbidity rates, increases in compound hot events over urban areas have extremely important implications for human health.

1. Introduction

As the global warming trend continues, extreme hot events have become more frequent in recent years (Meehl & Tebaldi, 2004; Perkins et al., 2012), which poses great threats to ecosystem services, food security, and human health (Easterling et al., 2000; Frölicher et al., 2018; He et al., 2018; Zeng et al., 2014). Meanwhile, urban heat islands (UHIs), which refer to the microclimatic phenomenon that urban areas are typically hotter than their surrounding rural areas, can further deteriorate the thermal environment in cities (Arnfield, 2003; S. Grimmond, 2007; Li & Bou-Zeid, 2013; L. Zhao et al., 2018). Despite that urban areas only account for 0.5% of land surface over globe (Y. Zhou et al., 2015), over 50% of the world's population live in cities today and by 2050 this number will rise up to 70% (Esch et al., 2017; K. W. Oleson et al., 2011). In China, which is the focus of this study, the urban population is expected to grow up to 80% by 2050 according to the National Bureau of Statistics (Yan et al., 2016). As a result of these ongoing trends, it is important to understand the vulnerability of urban residents to hot extremes and UHIs.

Previous studies often focused on the large-scale changes of hot extremes under climate change and did not separate urban and rural hot extremes (Baldwin et al., 2019; Y. Chen & Zhai, 2017; Easterling et al., 2000; Su & Dong, 2019; Sun et al., 2014; J. Wang et al., 2020). For instance, Y. Chen and Zhai (2017) analyzed the trends of summertime hot extremes in China based on observational data, and found that the frequency, intensity, and spatial extent of hot extremes are significantly increased during 1961–2015. Su and Dong (2019) and J. Wang et al. (2020) demonstrated that the anthropogenic forcing from rising greenhouse gases plays

a predominant role in controlling these increasing trends. On the other hand, many studies that did investigate the impacts of urbanization focused on the mean temperatures, not hot extremes. For example, observational studies have shown that urbanization can accelerate the increase of mean surface warming in China (Lin et al., 2016; Ren et al., 2008; Sun et al., 2016; Yang et al., 2011).

The UHI effect is expected to induce more hot extremes in urban areas because it shifts the mean of urban temperature distribution (Luo & Lau, 2018). Our recent research further shows that the shape of UHI distribution is also important in determining the contribution of urbanization to the trends of hot extremes. We found that the contribution of urbanization to the trends of hot extremes is stronger in wet climates due to a stronger increase in the mean UHI and also the smaller variability of UHI (Liao et al., 2018). Together these studies imply strong impacts of urbanization on hot extremes, which are confirmed by other observational studies in China (Ren & Zhou, 2014; Yang et al., 2017). Besides, using regional climate models coupled with urban canopy models (UCMs), many numerical studies also demonstrated that UHI effects can intensify heat extremes in cities (F. Chen et al., 2014; Liu et al., 2018; M. Wang et al., 2013). Recently, with the development of UCMs in Global Climate Models and Earth System Models, studies begin to quantify the combined urbanization and climate change effects on mean temperatures and hot extremes at continental to global scales (Li et al., 2016a; McCarthy et al., 2010; K. Oleson, 2012).

In this study, we use the Geophysical Fluid Dynamics Laboratory (GFDL) land model LM4.0, coupled with a newly developed UCM (LM4.0-UCM), to quantify changes in summertime hot extremes in China under two different representative concentration pathway (RCP) scenarios. The model was previously evaluated using three urban flux sites, and was used to study UHIs over the Contiguous United States (Li et al., 2016a, 2016b). Here, we evaluate the model performance in China based on a homogenized observational data set drawn from nearly 2,000 meteorological stations, and then examine the simulated changes in the three types of summertime hot extremes over both urban and rural land.

2. Materials and Methods

2.1. Meteorological Observations and Model Simulations

Meteorological observations, including daily maximum surface air temperature (T_{max}) and daily minimum surface air temperature (T_{min}) from 2,474 national stations in China for the summer season (i.e., May to September) of 1961–2000 are used in this study. The raw data set has been quality-controlled and homogenized using the method suggested by Xu et al. (2013). Stations are excluded if there are five or more missing days in any of the summer seasons, which leaves a total of 1,964 stations for subsequent analyses. Similar to previous studies, we dynamically classify meteorological stations into urban and rural stations based on time varying land-use/land-cover data in 1980, 1990, 1995, and 2000 (Liao et al., 2017, 2018). Stations with 33% or larger built-up fractions, which are calculated as the proportion of built-up area within circular buffers with a 2-km radius, are classified as urban stations, otherwise as rural stations.

The simulation model used in this study is the GFDL land model LM4.0 (Milly et al., 2014; Shevliakova et al., 2009), coupled with a newly developed and validated UCM (Li et al., 2016a, 2016b). Within each grid cell, LM4.0 represents different land-use/land-cover types (i.e., natural vegetation, secondary vegetation, grassland, pasture, and urban) as a collection of tiles (Held et al., 2019; Milly et al., 2014; Shevliakova et al., 2009; M. Zhao et al., 2018). One unique feature of the GFDL land model is that it can handle the transition between non-urban and urban tiles, thereby simulating the growth of urban areas that is critical for long-term climate simulations (see Li et al., 2016a). Like many other single-layer UCMs (Best & Grimmond, 2015; C. S. B. Grimmond et al., 2011), the UCM coupled with LM4.0 is built on the concept of an urban canyon and parameterizes important radiation processes including sky-view factors, shadow effects, and multiple reflections between walls and ground surfaces. It solves the surface energy balance equations for different urban facets, including the roof, the wall, the impervious ground, and the pervious ground. However, unlike UCMs that handle urban vegetation and impervious surfaces separately through a tiling approach (e.g., the single-layer UCM in the Weather Research and Forecasting model, see F. Chen et al., 2011), the UCM used in this study explicitly includes urban vegetation within the canyon, which interacts with impervious surfaces and the canyon air. The urban vegetation dynamics are further handled by a dynamic vegetation module (Shevliakova et al., 2009).

In this study, the LM4.0 coupled with the UCM is driven by atmospheric forcing from GFDL earth system model outputs (hereafter the GFDL forcing) or gridded data sets based on observations and reanalysis fields (hereafter the Sheffield forcing). The GFDL forcing refers to outputs from coupled land-atmosphere-ocean earth system model simulations for the Coupled Model Intercomparison Project Phase 5 (CMIP5) (Dunne et al., 2012, 2013), which did not use any UCM. Specifically, the 3-hourly, 2 by 2.5° ESM2Mb model outputs in the historical period and under RCP 2.6 and RCP 8.5 scenarios are used (Malyshev et al., 2015). The Sheffield forcing refers to the 50 year (1949–2000), 3-hourly, 1° data set, which is based on a combination of observational and reanalysis data (Sheffield et al., 2006). The simulations are similar to those presented in Gu and Li (2018) and Li et al. (2016b, 2019) but cover the entire globe. Specifically, we use the Sheffield forcing to conduct a simulation in the period of 1949–2000, which will be compared to observations to assess the model performance. For this simulation, we recycle the first 30 year forcing to the period of 1700–1948 in order to spin-up the land model. To examine future changes in hot extremes, we conduct another simulation from 1700 to 2100 using the GFDL forcing. In this simulation, no bias correction is applied to the GFDL forcing; nor is the so-called pseudo-global warming or the delta change method applied to the GFDL forcing (Ji et al., 2020; Yang et al., 2019). Nonetheless, it is sufficient for our research purpose since we only focus on changes in hot extremes in the simulation with the GFDL forcing, not the absolute magnitude. Given the difference in the resolutions of the two forcing data sets, we use a grid resolution of 2 by 2.5° for a consistent comparison. For analysis, we focus on the historical period from 1961 to 2000 and the future period from 2061 to 2100.

For the model simulations, the reference temperature reported at 2-m above the displacement height (Malyshev et al., 2015) is used. For each grid cell, the rural temperature is the area-average of all non-urban (i.e., natural vegetation, secondary vegetation, grassland, and pasture) 2-m temperatures. For observations, we average data from all urban (rural) stations within each grid cell to derive the grid averages of observed urban (rural) temperatures. When comparing modeled and observed temperatures, only 2° × 2.5° latitude-longitude grid cells containing at least one urban station and one rural station in the period 1980–2000 and with urban fractions larger than 0.1% in simulations are examined here (Figure S1). As a result, 91 grid cells are available for the evaluation.

2.2. Definition of Hot Extremes

There is no consensus on the definition of hot extremes and most previous studies used the daily maximum temperature or daily mean temperature to define hot extremes (Anderson & Bell, 2011; Meehl & Tebaldi, 2004; Peng et al., 2011). Recent studies have shown that the significant UHI effects at night often preclude the night-time relief of excessively hot temperatures in urban areas (Liao et al., 2017; Ren & Zhou, 2014). As a result, urban residents experience continuous high-intensity heat stress during the day and night, which lead to high mortality and morbidity rates (Hansen et al., 2008). In order to better capture the impact of hot extremes on human health, we define hot extreme events using both T_{max} and T_{min} following the study of Y. Chen and Zhai (2017) and we define them for urban and rural land separately.

Specifically, we divide hot extreme events into three types: independent hot day (IHD), independent hot night (IHN), and compound hot event (CHE). The 90th percentiles ($P^{90}_{max}/P^{90}_{min}$) of T_{max}/T_{min} during the base period (1961–1990) in the rural land are used as the thresholds. For each calendar day in the summer season (i.e., May to September), the $P^{90}_{max}/P^{90}_{min}$ is calculated from multiyear sample units of a 15-day moving window for the specific day over the base period (Y. Chen & Zhai, 2017; Yang et al., 2017). Here a day is defined as a 24-h period starting from 00 UTC. Given that in our study domain the local time is ahead of UTC by 8 h, the T_{max} typically appears before the T_{min} within a day. An IHD is then defined as a day with T_{max} exceeding P^{90}_{max} but the following T_{min} lower than P^{90}_{min}. An IHN is defined as a day with T_{max} lower than P^{90}_{max} but the following T_{min} exceeding P^{90}_{min}. A CHE is defined as a day with both T_{max} and the following T_{min} exceeding their corresponding P^{90}_{max} and P^{90}_{min}.

Based on this definition, each summer day is classified into IHD, IHN, CHE, or a non-hot extreme day. Three indicators, which are calculated at the annual scale for each grid cell, are used to describe the characteristics of hot extremes. The *frequency* measures the sum of hot extreme days. If two consecutive days were classified as the same type of hot extremes (e.g., IHD), then they are accounted as 2 days for the frequency indicator instead of 1. The *duration* measures the average length of consecutive hot extreme days. Given

that the smallest unit is 1 day, the duration will be equal to 1 if none of the hot extreme days were consecutive and will be always larger than 1 if there were consecutive hot extreme days. The *intensity* measures the average magnitude of hot extreme days, which is defined as temperature departure from its corresponding threshold. Specially, the intensity of CHEs is calculated as half of the sum of T_{max} and T_{min} minus their corresponding P^{90}_{max} and P^{90}_{min}. We then construct urban and rural time series of these hot extreme indicators by averaging their values across the 91 grid cells.

3. Results and Discussion

3.1. Evaluation of the Model Performance

To assess the model performance, we first compare the simulated urban and rural temperatures with the Sheffield forcing to the observed temperatures from meteorological stations. The comparison between observed and simulated probability density functions (PDFs) of spatially averaged urban and rural temperatures (daily T_{max} and T_{min}) is shown in Figure 1. Generally, both urban and rural temperatures are underestimated in model simulations for daily T_{max} and T_{min}. The mean values of observed urban (rural) daily T_{max} and T_{min} are 27.5°C and 17.0°C (26.7°C and 16.1°C), respectively, while the mean values of modeled urban (rural) daily T_{max} and T_{min} are 26.6°C and 15.4°C (26.5°C and 15.1°C). Nevertheless, the results from the two-sample Kolmogorov-Smirnov test (Massey, 1951), which are used to verify whether two PDF curves are from the same continuous distribution, suggest that the shapes of their corresponding PDF curves are similar between observations and simulations. In addition, the annual averages of modeled urban and rural temperatures are highly correlated with those of the observed ones (not shown). The correlation coefficients between the annual averages of modeled and observed T_{max} are 0.95 and 0.96 for urban and rural land, respectively; while those between the annual averages of modeled and observed T_{min} are 0.97 and 0.94 for urban and rural land, respectively. The high correlation coefficients indicate that the model captures the inter-annual variability of the temperature series, despite some biases in the mean values. This is partly thanks to the prescribed forcing derived from observations and reanalysis fields. Although model simulations underestimate the UHI intensities, the model captures that the impacts of urbanization on T_{min} are larger than T_{max}, which is consistent with the traditional paradigm that surface air UHIs are primarily a nighttime phenomenon (Oke et al., 2017) and the findings of many previous studies (Liao et al., 2017, 2018; Ren & Zhou, 2014; L. Zhou et al., 2004). Furthermore, we correct the modeled temperature series by removing the mean bias between observations and simulations, then compare the hot extremes, including their temporal variability and spatial patterns (Figures S2–S6). Generally, characteristics of hot extremes in rural land are better captured by the model than their counterparts in urban land. Nevertheless, the simulations can predict the impacts of urbanization on hot extremes, and capture the trends of occurrences of hot extremes in space (e.g., increases of frequency of IHNs and CHEs mainly occur in the eastern China).

Overall, these results indicate that despite some biases (especially in terms of the mean values), the GFDL land model LM4.0 coupled with the newly developed UCM in this study is able to capture the PDFs and inter-annual variations of T_{max} and T_{min} and characteristics of hot extremes reasonably well in both urban and rural areas. Based on this urbanized global earth system model, in the following sections, we analyze how summertime hot extremes change under different emission scenarios.

3.2. Changes in Summer-Mean Daily T_{max} and T_{min}

After evaluating the model performance, we use the simulated urban and rural temperatures with the GFDL forcing to explore changes of summertime hot extremes from history to future under different scenarios. It should be noted that since we do not apply any bias correction to the simulation results with the GFDL forcing, we will primarily focus on the changes in temperatures and hot extremes relative to the historical period rather than the absolute magnitude. In general, the occurrence of hot extreme events can be altered by a shift of the mean of the temperature PDF, and/or a change in the shape of the temperature PDF such as its width (Barnston et al., 2020; Liao et al., 2018; Schär et al., 2004). As the $P^{90}_{max}/P^{90}_{min}$ is calculated using rural temperatures, the UHI effect also contributes to the increase of hot extremes over the urban land. Hence, before analyzing summertime hot extremes, we examine the summer-mean urban and rural temperatures, as well as their differences (i.e., the summer-mean UHI intensities; Figure 2). As can be seen, both urban

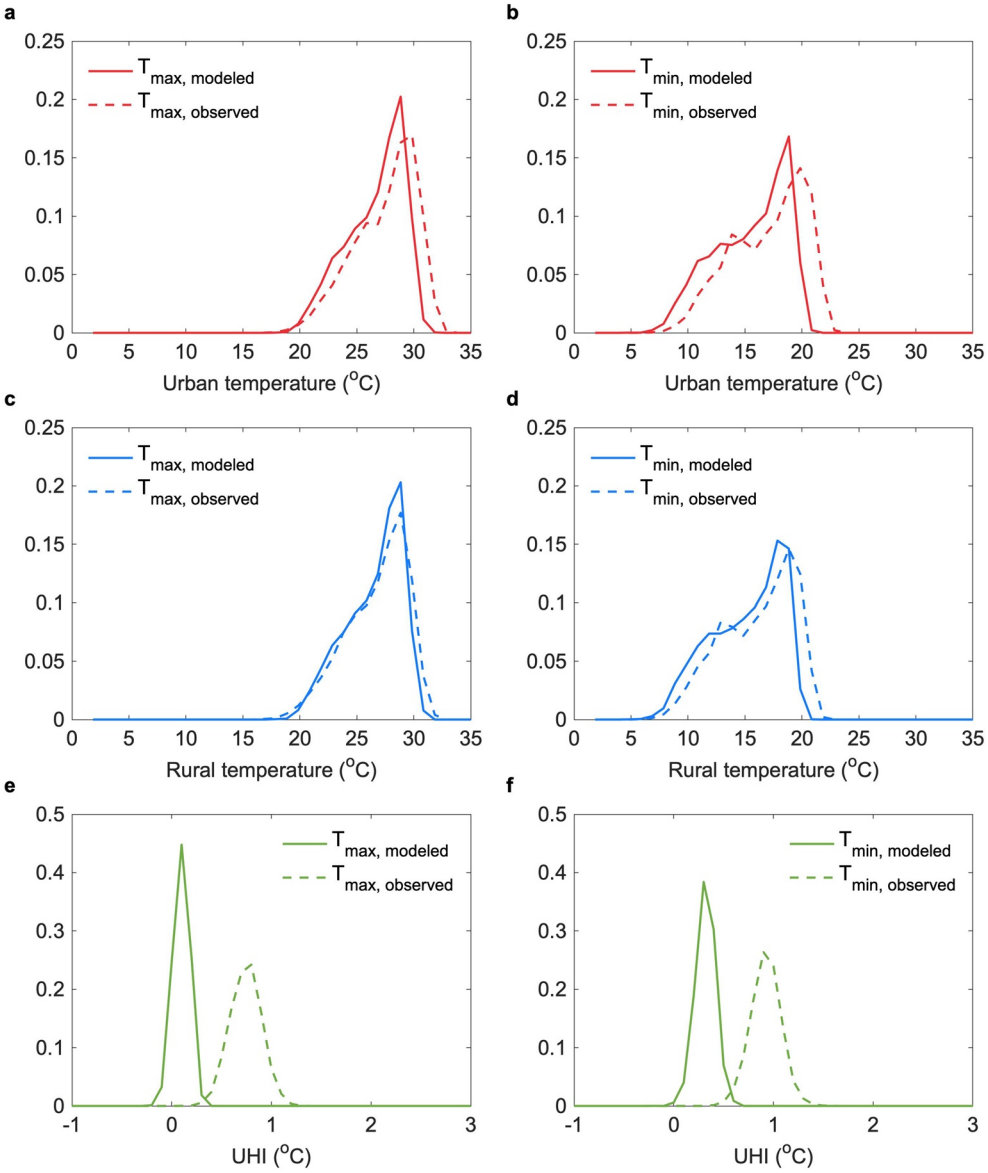

Figure 1. Probability density functions (PDFs) of spatially averaged daily maximum and minimum temperatures during the summer periods of 1961–2000 in China. (a) and (b) Results in urban areas and (c) and (d) are results in rural areas. (e) and (f) PDFs of urban heat island (UHI) intensities. These temperature variables are spatially averaged over China. The left panels show results calculated by daily maximum temperatures, and the right panels show results calculated by daily minimum temperatures. The dashed curves show results calculated by meteorological observations, and the solid curves show simulated results with the Sheffield forcing.

and rural temperatures (both T_{max} and T_{min}) show rising trends (Table S1), and, as expected, the increasing trends under the RCP 8.5 scenario are larger than those under the RCP 2.6 scenario. The summer-mean UHI intensities are positive and thus contribute to more hot extremes in the urban land. Moreover, the UHI intensities defined using T_{min} are about 3 times as larger as those defined using T_{max}. The stronger impact of urbanization on T_{min} has important implications for its unequal impacts on the three types of hot extremes, to be discussed later. Nevertheless, the summer-mean UHI intensities show insignificant or very small trends in both historical and future periods.

While the means of PDFs for both T_{max} and T_{min} in urban and rural land shift toward higher values, their width (represented by the standard deviation) shows no obvious changes (Figure S7 and Table S2). With the mean values shifting toward higher values and no changes in standard deviations, the occurrences of

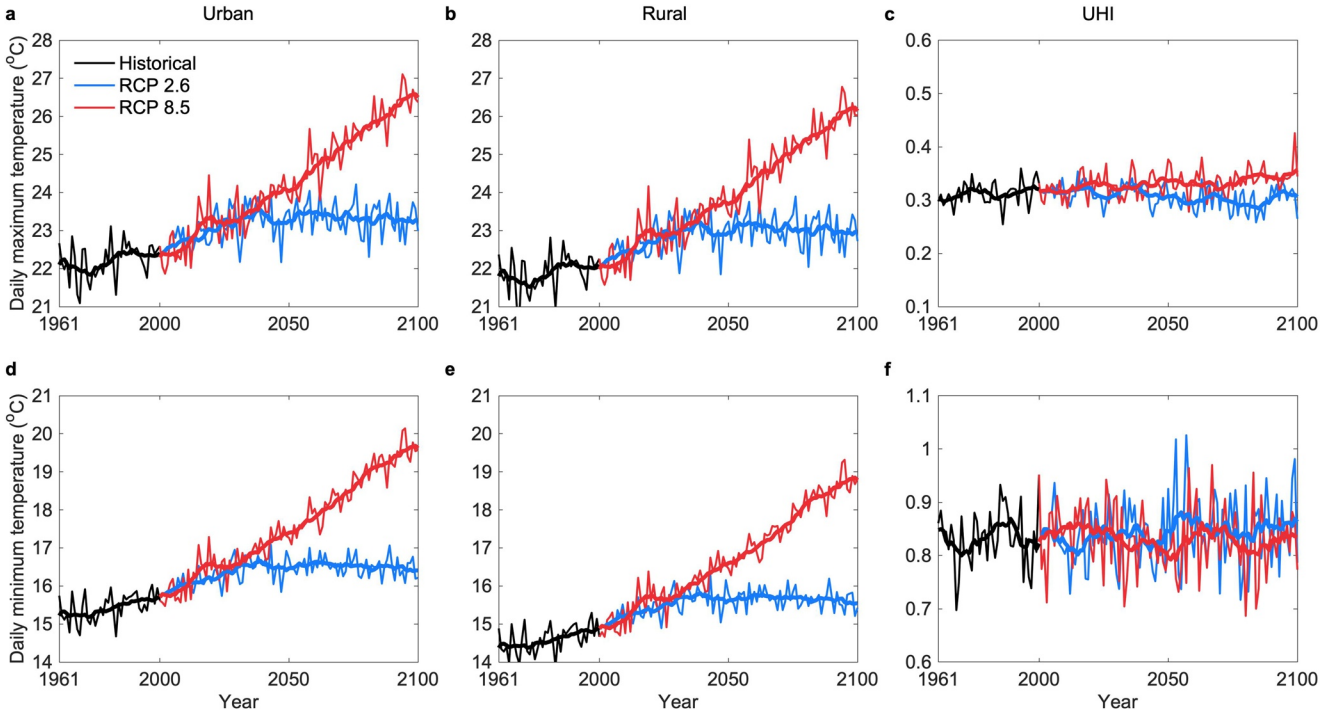

Figure 2. Summer-mean urban and rural temperatures under RCP 2.6 and RCP 8.5 scenarios in China. The top panels (a)–(c) show the daily maximum temperatures, and the bottom panels (d)–(f) show the daily minimum temperatures. The first column shows the urban temperatures, the second column shows the rural temperatures, and the third column shows the urban heat island (UHI) intensities. The solid curves denote the 10-year moving averages.

extreme values (i.e., hot days and hot nights) will inevitably increase. However, it remains unclear whether the increases in hot days (nights) will be manifested as independent hot days (nights) or compound events, which is examined in the following section.

3.3. Changes in Hot Extremes

Figure 3 shows the increases in the occurrence for IHDs, IHNs, and CHEs in urban and rural land, as well as the differences between urban and rural land, under two RCP scenarios. In terms of the IHD occurrences over the urban (rural) land, they increase from 7.7 (8.5) days per year over 1961–2000 to 9.1 (11.2) days per year over 2061–2100 under the RCP 2.6 scenario, and to 8.4 (12.1) days per year under the RCP 8.5 scenario. These results suggest that, as warming continues, the increases in the IHD occurrence in rural land are more rapidly than those in urban land, especially under the RCP 8.5 scenario (Table S3). As a result, their differences (i.e., urban minus rural) are negative and have significantly decreasing trends of −0.081 days/year/decade ($p < 0.05$) under the RCP 2.6 scenario and −0.375 days/year/decade ($p < 0.01$) under the RCP 8.5 scenario (Figure 3c), which, in space, mainly occurs in the northern part of China (Figures S8 and S9). It is noted that some previous studies examined the difference in urban and rural trends (e.g., Luo & Lau, 2018), instead of the trend of urban-rural difference shown here. We also compute the difference in urban and rural trends. Although there are minor changes in the computed values and their significance levels, the main findings are the same when using the difference in urban and rural trends.

The occurrences of IHNs are also increased. Specifically, the urban (rural) occurrences of IHN increase from 13.0 (8.5) days per year over 1961–2000 to 22.8 (17.2) days per year over 2061–2100 under the RCP 2.6 scenario and to 33.7 (30.4) days per year over 2061–2100 under the RCP 8.5 scenario. In contrast to IHDs, the urban-rural differences of IHN occurrences are positive, suggesting that IHNs occur more frequently in urban land. This is again consistent with the traditional paradigm that the UHI defined using surface air temperature is a primarily nighttime phenomenon (Oke et al., 2017) and the results in Figure 2. Their differences have an insignificantly increasing trend of +0.022 days/year/decade under the RCP 2.6 scenario but a rapidly decreasing trend of −0.398 days/year/decade ($p < 0.01$) under the RCP 8.5 scenario (Figure 3f),

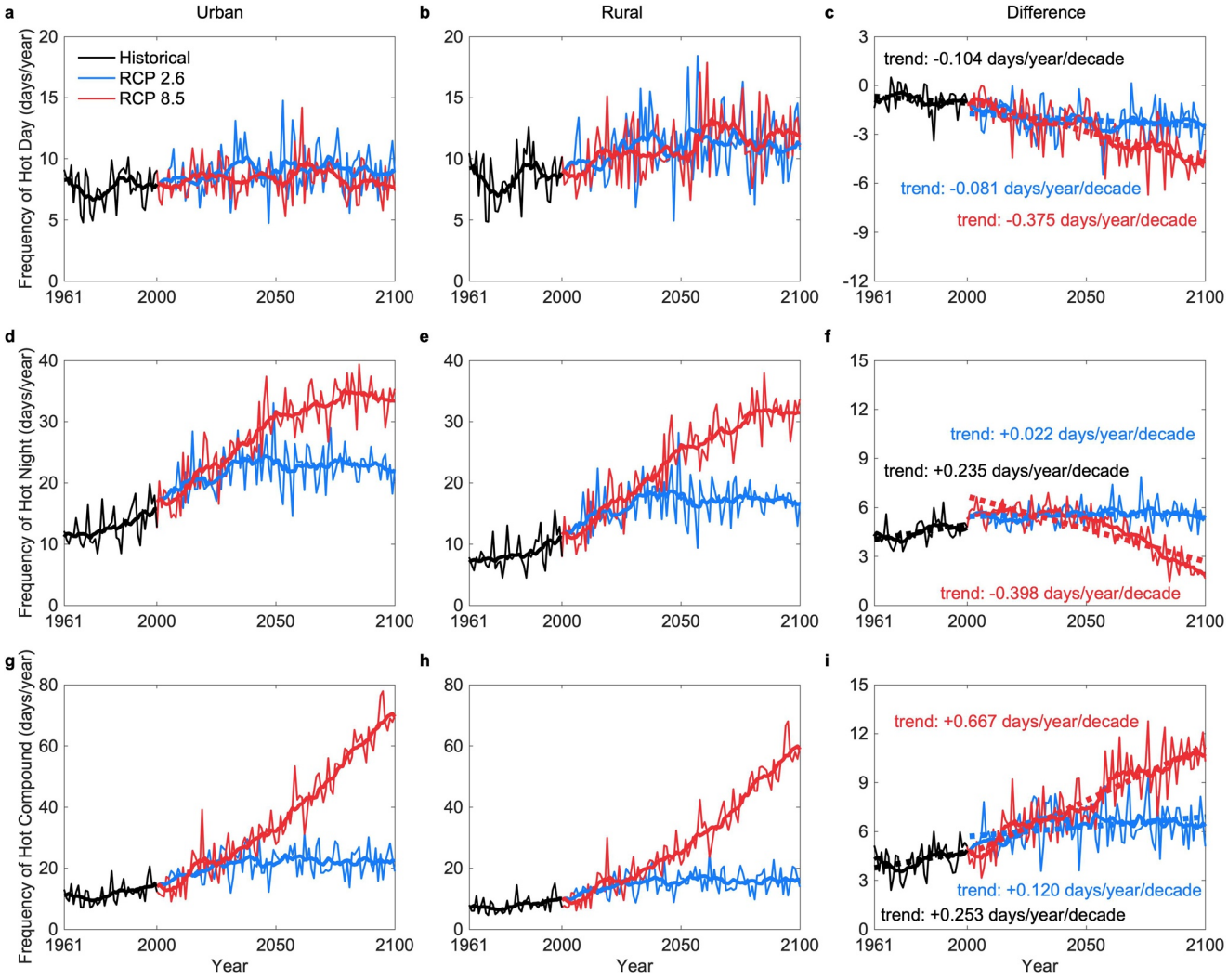

Figure 3. Urban and rural occurrences of summertime hot extremes under RCP 2.6 and RCP 8.5 scenarios in China. (a)–(c) Frequency of independent hot days in urban, rural, and their difference. (d)–(f) Frequency of independent hot nights in urban, rural, and their difference. (g)–(i) Frequency of compound hot events in urban, rural, and their difference. The first column shows the frequency in urban land, the second column shows the frequency in rural land, and the third column shows their differences. The solid curves denote the 10-year moving averages, and the dashed lines in the third column are linear regression fits.

which, in space, mainly occurs in the southeastern part of China (Figure S9). The decreasing trend of urban-rural differences in the occurrence of IHNs under the RCP 8.5 scenario is related to the increasing trend of urban-rural differences in the occurrence of CHEs, to be discussed below, because the three types of hot extremes are mutually exclusive.

Different from the IHD and IHN events, the urban and rural occurrences of CHEs are consistently increased under the two different emission scenarios and the increases under the RCP 8.5 scenario are markedly stronger than those under the RCP 2.6 scenario (Figure 3i). Urban (rural) occurrences of CHEs increase from 11.8 (8.0) days per year over 1961–2000 to 22.3 (16.0) days per year over 2061–2100 under the RCP 2.6 scenario and 56.1 (46.0) days per year over 2061–2100 under the RCP 8.5 scenario. Generally, increases of CHEs over urban land are faster than those over rural land in the eastern part of China (Figure S9). As a result, at the end of this century, CHEs are projected to be the dominant type in both urban and rural land under the RCP 8.5 scenario.

Figure 4 further shows the proportions of IHDs, IHNs, and CHEs in the historical period of 1961–2000 and the future period of 2061–2100 under RCP 2.6 and RCP 8.5 scenarios. It is clear that not only do the total

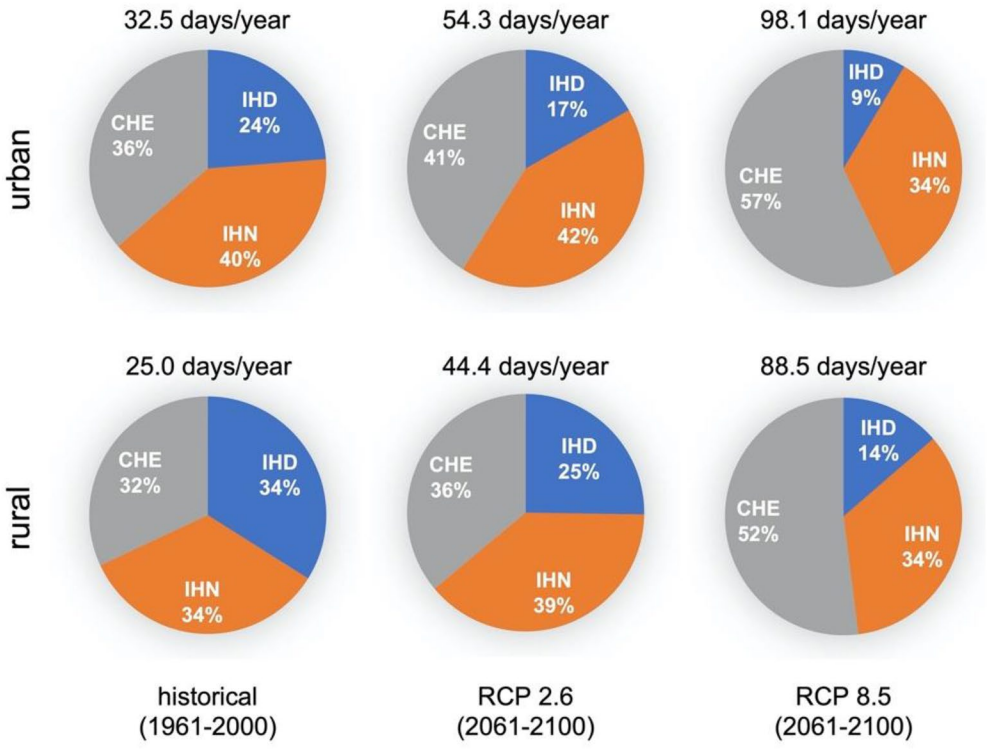

Figure 4. Changes in the proportions of independent hot days, independent hot nights, and compound hot events. The top panels show the proportions of the three types of extreme hot events changing from the historical period of 1961–2000 (the first column) to the future period of 2061–2100 under the RCP 2.6 (the second column), and RCP 8.5 (the third column) scenarios in urban land, and the bottom panels show the results in rural land. The values on top of each pie show the annual average of the total occurrence for the three types of extreme hot events.

occurrences of extreme hot events continue to increase (Figure 3), their proportions also change. The proportion of IHDs in urban (rural) land decreases from 24% (34%) over 1961–2000 to 17% (25%) over 2061–2100 under the RCP 2.6 scenario and to 9% (14%) over 2061–2100 under the RCP 8.5 scenario. The proportion of IHNs in urban (rural) land increases from 40% (34%) over 1961–2000 to 42% (39%) over 2061–2100 under the RCP 2.6 scenario but decreases to 34% (no change) over 2061–2100 under the RCP 8.5 scenario. In contrary, the proportion of CHEs in urban (rural) land increases from 36% (32%) over 1961–2000 to 41% (36%) over 2061–2100 under the RCP 2.6 scenario and to 57% (52%) over 2061–2100 under the RCP 8.5 scenario. These results demonstrate that, as climate warms, hot extremes will gradually transition to more compound events than independent extremes and this transition is stronger in urban land than that in rural land.

Why does the CHE proportion increase in the future and why is the increase stronger in urban land than in rural land? Given that the $P^{90}_{max}/P^{90}_{min}$ is calculated using temperatures (more specifically the rural temperatures) in the historical period, the shifts of mean T_{max} and T_{min} toward higher values as the climate warms will lead to more hot days and hot nights, respectively. With more hot days and hot nights, compound extremes will inevitably increase as the independent events would more likely become connected. While the increase of compound extremes could be also caused by an increase in the cross-correlation between T_{max} and T_{min}, we found no such increases in the cross-correlation (Figure S10), suggesting that the increase of compound extremes is more caused by the increases of mean temperatures rather than the increases of correlations. This is consistent with a previous study (Baldwin et al., 2019), although that study did not separate urban and rural hot extremes. For similar reasons, the positive UHI effects can be viewed as shifting the mean urban temperatures toward higher values relative to the mean rural temperatures, thus causing the CHE to increase even more strongly in urban land than in rural land.

Figure S11 shows the changes in the duration of IHDs, IHNs, and CHEs in urban, rural, and their differences. Recall that the duration is the average length of consecutive hot extreme days. The average length of IHDs in urban land (1.4 days) is slightly shorter than that in rural land (1.5 days) during the historical period, and there are no significant trends under different scenarios (Table S4). In contrast with IHDs, the average length of IHNs in urban land (1.6 days) is slightly longer than that in rural land (1.5 days) during the historical period. Additionally, the average duration of IHNs increases under different scenarios. This increasing rate in urban land is slower than that in rural land under the RCP 8.5 scenario but faster under the RCP 2.6 scenario. For CHEs, the average length in urban land (2.0 days) is longer than that in rural land (1.7 days) during the historical period. The average duration of CHEs increases in both urban and rural land and the urban-rural differences also gradually increase in the future. Overall, these results suggest that, as warming continues, the average duration of IHNs and CHEs will be also longer in the future. With the impacts of urbanization, their average length in urban land is consistently longer than that in rural land, and for CHEs their differences will significantly increase under the RCP 8.5 scenario.

Similarly, Figure S12 shows the intensity changes of IHDs, IHNs, and CHEs in urban, rural, and their differences under RCP 2.6 and RCP 8.5 scenarios. As T_{max} or T_{min} increases, the average intensities of all extreme hot events in both urban and rural land experience different levels of rise. For the average intensity of IHDs, its value in urban land is smaller than that in rural land, and its increasing rate in urban land is close to that in rural land (Table S5). For the intensity of IHNs, its value in urban land is larger than that in rural land, and their differences have a weakly increasing trend of +0.0004°C/decade under the RCP 2.6 scenario but a significantly increasing trend of +0.005°C/decade under the RCP 8.5 scenario. The intensity of CHEs in urban land is also larger than that in rural land, and their differences have an insignificantly decreasing trend of −0.002°C/decade under the RCP 2.6 scenario but a strongly increasing trend of +0.011°C/decade under the RCP 8.5 scenario. Generally, changes of the intensity of these three types of summertime hot extremes are smaller under the RCP 2.6 scenario and larger under the RCP 8.5 scenario. In particular, the urban impacts are the strongest on CHEs under the RCP 8.5 scenario.

Our finding that the frequencies and intensities of IHNs and CHEs increase during the historical period is consistent with the results in the study by Y. Chen and Zhai (2017). However, they did not quantify the changes of these hot extremes in urban and rural land separately. Our results show that the increasing rates of IHNs and CHEs in urban areas are faster than those over rural areas during the historical period (Figure 3 and Table S3). Furthermore, we show that as warming continues, both urban and rural land see more CHEs and the frequency, duration, and intensity of CHEs increase more strongly in urban land than those in rural land. In this sense, urbanization accelerates the transition of hot extremes from daytime-/nighttime-only events to compound events. As more and more studies have demonstrated that consecutive hot periods without limited nighttime relief will significantly increase mortality and morbidity rates (Gasparrini et al., 2015; Guo et al., 2017; Hansen et al., 2008), the faster increases in the frequency, duration, and intensity of CHEs in urban areas highlights the urgency of developing and implementing mitigation and adaptation strategies to combat the adverse health effects of global warming and UHI.

4. Conclusions

Using the GFDL land model LM4.0 coupled with a newly developed UCM and treating urban and rural land as subgrid units, urban-rural temperature differences under the present-day climate and two future scenarios in China are simulated in this study. To evaluate the model performance, we use temperatures observed at nearly 2,000 meteorological stations. The results show that the model can capture the changes and variabilities of T_{max} and T_{min}, and the urbanization effects on surface air temperature reasonably well. As expected, the temperatures in both urban and rural areas show increasing trends under RCP 2.6 and RCP 8.5 scenarios. However, UHI intensities show no obvious changes.

Following recent studies, we categorize summertime hot extremes into three types, that is, IHD, IHN, and CHE (Y. Chen & Zhai, 2017; Y. Chen et al., 2018). Our simulations show that, as warming continues, all three kinds of summertime hot extremes will become more frequent, longer lasting, and more intense in the future. Moreover, hot extremes will gradually switch to more compound events than independent extremes,

and, importantly, this transition is even stronger in urban land. As a result, the increases of the CHEs in urban land are faster than those in rural land.

As the urban population continues to increase in the near future (Shi et al., 2020), this study highlights that effectively mitigating hot extremes in urban areas is particularly important. We caution that as our results are only drawn from the simulations with the GFDL model, the results can be affected by model uncertainties including those from parameterizations used in the UCM and strategies to represent subgrid surface heterogeneity in the land surface model (Lawrence et al., 2016). With new subgrid data from the CMIP6, results of multiple models coupled with UCMs can be used to quantify these uncertainties and inform risks of summertime hot extremes in urban areas in future studies.

Data Availability Statement

The meteorological data and land-use/land-cover maps are available at http://data.cma.cn/en/ and http://www.resdc.cn/Datalist1.aspx?FieldTyepID=1,3 (data only available in Chinese), respectively.

Acknowledgments
This study was supported by the National Key Research and Development Program of China (grants 2019YFA0607203 and 2017YFA0604404), the National Natural Science Foundation of China (grants 41901327 and 41871318), the Guangdong Basic and Applied Basic Research Foundation (grant 2019A1515010823), the Fundamental Research Funds for the Central Universities (grant 19lgpy41), the project funded by China Postdoctoral Science Foundation (grants 2020M672937 and 2020T130732). D. Li acknowledges support from the U.S. Army Research Office (grant W911NF-18-1-0360). The authors are thankful to the China Meteorological Data Service Center and the Data Center for Resources and Environmental Sciences of the Chinese Academy of Sciences for providing the meteorological data and land-use/land-cover maps.

References

Anderson, G. B., & Bell, M. L. (2011). Heat waves in the United States: Mortality risk during heat waves and effect modification by heat wave characteristics in 43 U.S. communities. *Environmental Health Perspectives*, *119*(2), 210–218.

Arnfield, A. J. (2003). Two decades of urban climate research: A review of turbulence, exchanges of energy and water, and the urban heat island. *International Journal of Climatology*, *23*(1), 1–26. https://doi.org/10.1002/joc.859

Baldwin, J. W., Dessy, J. B., Vecchi, G. A., & Oppenheimer, M. (2019). Temporally compound heat wave events and global warming: An emerging hazard. *Earth's Future*, *7*(4), 411–427. https://doi.org/10.1029/2018EF000989

Barnston, A. G., Lyon, B., Coffel, E. D., & Horton, R. M. (2020). Daily autocorrelation and mean temperature/moisture rise as determining factors for future heatwave patterns in the U.S. *Journal of Applied Meteorology and Climatology*, *59*, 1–62. https://doi.org/10.1175/JAMC-D-19-0291.1

Best, M. J., & Grimmond, C. S. B. (2015). Key conclusions of the first international urban land surface model comparison project. *Bulletin of the American Meteorological Society*, *96*(5), 805–819. https://doi.org/10.1175/BAMS-D-14-00122.1

Chen, F., Kusaka, H., Bornstein, R., Ching, J., Grimmond, C. S. B., Grossman-Clarke, S., et al. (2011). The integrated WRF/urban modeling system: Development, evaluation, and applications to urban environmental problems. *International Journal of Climatology*, *31*(2), 273–288. https://doi.org/10.1002/joc.2158

Chen, F., Yang, X., & Zhu, W. (2014). WRF simulations of urban heat island under hot-weather synoptic conditions: The case study of Hangzhou City, China. *Atmospheric Research*, *138*, 364–377. https://doi.org/10.1016/j.atmosres.2013.12.005

Chen, Y., & Zhai, P. (2017). Revisiting summertime hot extremes in China during 1961-2015: Overlooked compound extremes and significant changes. *Geophysical Research Letters*, *44*(10), 5096–5103. https://doi.org/10.1002/2016GL072281

Chen, Y., Zhai, P., & Zhou, B. (2018). Detectable impacts of the past half-degree global warming on summertime hot extremes in China. *Geophysical Research Letters*, *45*(14), 7130–7139. https://doi.org/10.1029/2018GL079216

Dunne, J. P., John, J. G., Adcroft, A. J., Griffies, S. M., Hallberg, R. W., Shevliakova, E., et al. (2012). GFDL's ESM2 Global Coupled Climate–Carbon Earth System Models. Part I: Physical formulation and baseline simulation characteristics. *Journal of Climate*, *25*(19), 6646–6665. https://doi.org/10.1175/JCLI-D-11-00560.1

Dunne, J. P., John, J. G., Shevliakova, E., Stouffer, R. J., Krasting, J. P., Malyshev, S. L., et al. (2013). GFDL's ESM2 Global Coupled Climate–Carbon Earth System Models. Part II: Carbon System formulation and baseline simulation characteristics. *Journal of Climate*, *26*(7), 2247–2267. https://doi.org/10.1175/JCLI-D-12-00150.1

Easterling, D. R., Meehl, G. A., Parmesan, C., Changnon, S. A., Karl, T. R., & Mearns, L. O. (2000). Climate extremes: Observations, modeling, and impacts. *Science*, *289*(5487), 2068–2074.

Esch, T., Heldens, W., Hirner, A., Keil, M., Marconcini, M., Roth, A., et al. (2017). Breaking new ground in mapping human settlements from space – The Global Urban Footprint. *ISPRS Journal of Photogrammetry and Remote Sensing*, *134*, 30–42. https://doi.org/10.1016/j.isprsjprs.2017.10.012

Frölicher, T. L., Fischer, E. M., & Gruber, N. (2018). Marine heatwaves under global warming. *Nature*, *560*(7718), 360–364. https://doi.org/10.1038/s41586-018-0383-9

Gasparrini, A., Guo, Y., Hashizume, M., Lavigne, E., Zanobetti, A., Schwartz, J., et al. (2015). Mortality risk attributable to high and low ambient temperature: A multicountry observational study. *The Lancet*, *386*(9991), 369–375.

Grimmond, C. S. B., Blackett, M., Best, M. J., Baik, J. J., Belcher, S. E., Beringer, J., et al. (2011). Initial results from Phase 2 of the international urban energy balance model comparison. *International Journal of Climatology*, *31*(2), 244–272.

Grimmond, S. (2007). Urbanization and global environmental change: Local effects of urban warming. *Geographical Journal*, *173*(1), 83–88. https://doi.org/10.1111/j.1475-4959.2007.232_3.x

Gu, Y., & Li, D. (2018). A modeling study of the sensitivity of urban heat islands to precipitation at climate scales. *Urban Climate*, *24*, 982–993. https://doi.org/10.1016/j.uclim.2017.12.001

Guo, Y., Gasparrini, A., Armstrong Ben, G., Tawatsupa, B., Tobias, A., Lavigne, E., et al. (2017). Heat wave and mortality: A multicountry, multicommunity study. *Environmental Health Perspectives*, *125*(8), 087006. https://doi.org/10.1289/EHP1026

Hansen, A., Bi, P., Nitschke, M., Ryan, P., Pisaniello, D., & Tucker, G. (2008). The effect of heat waves on mental health in a temperate Australian city. *Environmental Health Perspectives*, *116*(10), 1369–1375.

He, L., Cleverly, J., Wang, B., Jin, N., Mi, C., Liu, D. L., & Yu, Q. (2018). Multi-model ensemble projections of future extreme heat stress on rice across southern China. *Theoretical and Applied Climatology*, *133*(3), 1107–1118. https://doi.org/10.1007/s00704-017-2240-4

Held, I. M., Guo, H., Adcroft, A., Dunne, J. P., Horowitz, L. W., Krasting, J., et al. (2019). Structure and performance of GFDL's CM4.0 Climate Model. *Journal of Advances in Modeling Earth Systems*, *11*(11), 3691–3727. https://doi.org/10.1029/2019MS001829

Ji, P., Yuan, X., Ma, F., & Pan, M. (2020). Accelerated hydrological cycle over the Sanjiangyuan region induces more streamflow extremes at different global warming levels. *Hydrology and Earth System Sciences*, *24*, 5439–5451. https://doi.org/10.5194/hess-24-5439-2020

Lawrence, D. M., Hurtt, G. C., Arneth, A., Brovkin, V., Calvin, K. V., Jones, A. D., et al. (2016). The Land Use Model Intercomparison Project (LUMIP) contribution to CMIP6: Rationale and experimental design. *Geoscientific Model Development*, *9*(9), 2973–2998. https://doi.org/10.5194/gmd-9-2973-2016

Li, D., & Bou-Zeid, E. (2013). Synergistic interactions between urban heat islands and heat waves: The impact in cities is larger than the sum of its parts. *Journal of Applied Meteorology and Climatology*, *52*(9), 2051–2064. https://doi.org/10.1175/JAMC-D-13-02.1

Li, D., Liao, W., Rigden, A. J., Liu, X., Wang, D., Malyshev, S., & Shevliakova, E. (2019). Urban heat island: Aerodynamics or imperviousness? *Science Advances*, *5*(4), eaau4299.

Li, D., Malyshev, S., & Shevliakova, E. (2016a). Exploring historical and future urban climate in the Earth System Modeling framework: 2. Impact of urban land use over the Continental United States. *Journal of Advances in Modeling Earth Systems*, *8*(2), 936–953. https://doi.org/10.1002/2015MS000579

Li, D., Malyshev, S., & Shevliakova, E. (2016b). Exploring historical and future urban climate in the Earth System Modeling framework: 1. Model development and evaluation. *Journal of Advances in Modeling Earth Systems*, *8*(2), 917–935. https://doi.org/10.1002/2015MS000578

Liao, W., Liu, X., Li, D., Luo, M., Wang, D., Wang, S., et al. (2018). Stronger contributions of urbanization to heat wave trends in wet climates. *Geophysical Research Letters*, *45*(20), 11310–11317. https://doi.org/10.1029/2018GL079679

Liao, W., Wang, D., Liu, X., Wang, G., & Zhang, J. (2017). Estimated influence of urbanization on surface warming in Eastern China using time-varying land use data. *International Journal of Climatology*, *37*(7), 3197–3208. https://doi.org/10.1002/joc.4908

Lin, S., Feng, J., Wang, J., & Hu, Y. (2016). Modeling the contribution of long-term urbanization to temperature increase in three extensive urban agglomerations in China. *Journal of Geophysical Research: Atmospheres*, *121*(4), 1683–1697. https://doi.org/10.1002/2015JD024227

Liu, X., Tian, G., Feng, J., Ma, B., Wang, J., & Kong, L. (2018). Modeling the warming impact of urban land expansion on hot weather using the weather research and forecasting model: A case study of Beijing, China. *Advances in Atmospheric Sciences*, *35*(6), 723–736. https://doi.org/10.1007/s00376-017-7137-8

Luo, M., & Lau, N. C. (2018). Increasing heat stress in urban areas of eastern China: Acceleration by urbanization. *Geophysical Research Letters*, *45*(23), 13060–13069. https://doi.org/10.1029/2018GL080306

Malyshev, S., Shevliakova, E., Stouffer, R. J., & Pacala, S. W. (2015). Contrasting local versus regional effects of land-use-change-induced heterogeneity on historical climate: Analysis with the GFDL Earth System Model. *Journal of Climate*, *28*(13), 5448–5469. https://doi.org/10.1175/JCLI-D-14-00586.1

Massey, F. J. (1951). The Kolmogorov-Smirnov test for goodness of fit. *Journal of the American Statistical Association*, *46*(253), 68–78.

McCarthy, M. P., Best, M. J., & Betts, R. A. (2010). Climate change in cities due to global warming and urban effects. *Geophysical Research Letters*, *37*(9), L09705. https://doi.org/10.1029/2010GL042845

Meehl, G. A., & Tebaldi, C. (2004). More intense, more frequent, and longer lasting heat waves in the 21st century. *Science*, *305*(5686), 994–997.

Milly, P. C. D., Malyshev, S. L., Shevliakova, E., Dunne, K. A., Findell, K. L., Gleeson, T., et al. (2014). An enhanced model of land water and energy for global hydrologic and earth-system studies. *Journal of Hydrometeorology*, *15*(5), 1739–1761. https://doi.org/10.1175/JHM-D-13-0162.1

Oke, T. R., Mills, G., Christen, A., & Voogt, J. A. (2017). *Urban climates*. Cambridge, MA. Cambridge University Press.

Oleson, K. (2012). Contrasts between urban and rural climate in CCSM4 CMIP5 climate change scenarios. *Journal of Climate*, *25*(5), 1390–1412. https://doi.org/10.1175/JCLI-D-11-00098.1

Oleson, K. W., Bonan, G. B., Feddema, J., & Jackson, T. (2011). An examination of urban heat island characteristics in a global climate model. *International Journal of Climatology*, *31*(12), 1848–1865. https://doi.org/10.1002/joc.2201

Peng, R. D., Bobb, J. F., Tebaldi, C., McDaniel, L., Bell, M. L., & Dominici, F. (2011). Toward a quantitative estimate of future heat wave mortality under global climate change. *Environmental Health Perspectives*, *119*(5), 701–706.

Perkins, S. E., Alexander, L. V., & Nairn, J. R. (2012). Increasing frequency, intensity and duration of observed global heatwaves and warm spells. *Geophysical Research Letters*, *39*, L20714. https://doi.org/10.1029/2012GL053361

Ren, G., & Zhou, Y. (2014). Urbanization effect on trends of extreme temperature indices of national stations over mainland China, 1961–2008. *Journal of Climate*, *27*(6), 2340–2360. https://doi.org/10.1175/JCLI-D-13-00393.1

Ren, G., Zhou, Y., Chu, Z., Zhou, J., Zhang, A., Guo, J., & Liu, X. (2008). Urbanization effects on observed surface air temperature trends in North China. *Journal of Climate*, *21*(6), 1333–1348. https://doi.org/10.1175/2007JCLI1348.1

Schär, C., Vidale, P. L., Lüthi, D., Frei, C., Häberli, C., Liniger, M. A., & Appenzeller, C. (2004). The role of increasing temperature variability in European summer heatwaves. *Nature*, *427*, 332–336. https://doi.org/10.1038/nature02300

Sheffield, J., Goteti, G., & Wood, E. F. (2006). Development of a 50-year high-resolution global dataset of meteorological forcings for land surface modeling. *Journal of Climate*, *19*, 3088–3111. https://doi.org/10.1175/JCLI3790.1

Shevliakova, E., Pacala, S. W., Malyshev, S., Hurtt, G. C., Milly, P. C. D., Caspersen, J. P., et al. (2009). Carbon cycling under 300 years of land use change: Importance of the secondary vegetation sink. *Global Biogeochemical Cycles*, *23*, GB2022. https://doi.org/10.1029/2007GB003176

Shi, Q., Liu, M., Liu, X., Liu, P., Zhang, P., Yang, J., & Li, X. (2020). Domain adaption for fine-grained urban village extraction from satellite images. *IEEE Geoscience and Remote Sensing Letters*, *17*(8), 1430–1434. https://doi.org/10.1109/LGRS.2019.2947473

Su, Q., & Dong, B. (2019). Recent decadal changes in heat waves over China: Drivers and mechanisms. *Journal of Climate*, *32*(14), 4215–4234. https://doi.org/10.1175/JCLI-D-18-0479.1

Sun, Y., Zhang, X., Ren, G., Zwiers, F. W., & Hu, T. (2016). Contribution of urbanization to warming in China. *Nature Climate Change*, *6*(7), 706–709. https://doi.org/10.1038/nclimate2956

Sun, Y., Zhang, X., Zwiers, F. W., Song, L., Wan, H., Hu, T., et al. (2014). Rapid increase in the risk of extreme summer heat in Eastern China. *Nature Climate Change*, *4*(12), 1082–1085. https://doi.org/10.1038/nclimate2410

Wang, J., Chen, Y., Tett, S. F. B., Yan, Z., Zhai, P., Feng, J., & Xia, J. (2020). Anthropogenically-driven increases in the risks of summertime compound hot extremes. *Nature Communications*, *11*(1), 528.

Wang, M., Yan, X., Liu, J., & Zhang, X. (2013). The contribution of urbanization to recent extreme heat events and a potential mitigation strategy in the Beijing–Tianjin–Hebei metropolitan area. *Theoretical and Applied Climatology*, *114*(3), 407–416. https://doi.org/10.1007/s00704-013-0852-x

Xu, W., Li, Q., Wang, X. L., Yang, S., Cao, L., & Feng, Y. (2013). Homogenization of Chinese daily surface air temperatures and analysis of trends in the extreme temperature indices. *Journal of Geophysical Research: Atmospheres*, *118*(17), 9708–9720. https://doi.org/10.1002/jgrd.50791

Yan, Z.-W., Wang, J., Xia, J.-J., & Feng, J.-M. (2016). Review of recent studies of the climatic effects of urbanization in China. *Advances in Climate Change Research*, *7*(3), 154–168. https://doi.org/10.1016/j.accre.2016.09.003

Yang, X., Hou, Y., & Chen, B. (2011). Observed surface warming induced by urbanization in east China. *Journal of Geophysical Research*, *116*, D14113. https://doi.org/10.1029/2010JD015452

Yang, X., Ruby Leung, L., Zhao, N., Zhao, C., Qian, Y., Hu, K., et al. (2017). Contribution of urbanization to the increase of extreme heat events in an urban agglomeration in east China. *Geophysical Research Letters*, *44*(13), 6940–6950. https://doi.org/10.1002/2017GL074084

Yang, X., Yu, X., Wang, Y., Liu, Y., Zhang, M., Ren, L., et al. (2019). Estimating the response of hydrological regimes to future projections of precipitation and temperature over the upper Yangtze River. *Atmospheric Research*, *230*, 104627.

Zeng, W., Lao, X., Rutherford, S., Xu, Y., Xu, X., Lin, H., et al. (2014). The effect of heat waves on mortality and effect modifiers in four communities of Guangdong Province, China. *Science of the Total Environment*, *482–483*, 214–221.

Zhao, L., Oppenheimer, M., Zhu, Q., Baldwin, J. W., Ebi, K. L., Bou-Zeid, E., et al. (2018). Interactions between urban heat islands and heat waves. *Environmental Research Letters*, *13*(3), 034003. https://doi.org/10.1088/1748-9326/aa9f73

Zhao, M., Golaz, J. C., Held, I. M., Guo, H., Balaji, V., Benson, R., et al. (2018). The GFDL Global Atmosphere and Land Model AM4.0/LM4.0: 2. Model description, sensitivity studies, and tuning strategies. *Journal of Advances in Modeling Earth Systems*, *10*(3), 735–769. https://doi.org/10.1002/2017MS001209

Zhou, L., Dickinson, R. E., Tian, Y., Fang, J., Li, Q., Kaufmann, R. K., et al. (2004). Evidence for a significant urbanization effect on climate in China. *Proceedings of the National Academy of Sciences of the United States of America*, *101*(26), 9540–9544.

Zhou, Y., Smith, S. J., Zhao, K., Imhoff, M., Thomson, A., Bond-Lamberty, B., et al. (2015). A global map of urban extent from nightlights. *Environmental Research Letters*, *10*(5), 054011. https://doi.org/10.1088/1748-9326/10/5/054011